metals

MDPI

Article

Thermodynamic Simulation Model of Copper Side-Blown Smelting Process

Mingzhou Li [1,2,*], Yuchen Feng [2] and Xinzhou Chen [2]

[1] Zijin Mining Group Co., Ltd., Longyan 361000, China
[2] School of Metallurgical Engineering, Jiangxi University of Science and Technology, Ganzhou 341000, China; 18629603252@163.com (Y.F.); 17816120480@163.com (X.C.)
* Correspondence: jxustlmz@jxust.edu.cn

Abstract: In this study, the thermodynamic simulation model and system of the copper side-blown smelting process were established using the chemical equilibrium constant method, based on the process reaction mechanism, multiphase equilibrium principle, and MetCal software platform (MetCal v7.81). Under typical production conditions, the composition of the product and the distribution behavior of impurity elements were simulated. The results indicate that the average relative error between the calculated mass fractions of major elements such as Cu, S, Fe, SiO_2, CaO, MgO, and Al_2O_3 in copper matte and smelting slag, and the actual production values, is 4.25%. Additionally, the average relative error between the calculated distribution ratios of impurity elements such as Pb, Zn, As, Bi, Mo, Au, and Ag in copper matte and smelting slag, and the actual production data, is 6.74%. Therefore, this model and calculation system accurately reflects the actual production situation of the copper side-blown smelting process well and has potential to predict process output accurately while optimizing process parameters, effectively guiding production practice.

Keywords: copper side-blown smelting; multiphase equilibrium; MetCal; thermodynamic simulation; mathematical model

Citation: Li, M.; Feng, Y.; Chen, X. Thermodynamic Simulation Model of Copper Side-Blown Smelting Process. *Metals* **2024**, *14*, 840. https://doi.org/10.3390/met14080840

Academic Editor: Mark E. Schlesinger

Received: 12 June 2024
Revised: 21 July 2024
Accepted: 21 July 2024
Published: 23 July 2024

1. Introduction

The side-blown smelting process is a modern and intensified new technology for copper smelting in a bath independently innovated by China [1]. It boasts advantages such as strong adaptability to raw materials, high production efficiency, low investment, low production costs, and environmental friendliness. It is also currently one of the preferred processes for treating complex lead-zinc ore, copper-bearing solid waste and hazardous waste, urban mines, and other difficult-to-treat secondary resources [2–4]. More than 20 production lines have been established in China, with an annual capacity of cathode copper accounting for more than 20%, demonstrating a promising application prospect. With the implementation of the national strategies of "carbon peaking and carbon neutrality" and "digitalization", the digital and intelligent transformation and upgrading of the copper smelting production process has become an important means to further improve quality and efficiency, as well as to conserve energy and reduce emissions.

However, the copper side-blown oxidation smelting process belongs to a complex pyrometallurgical reaction system that involves high temperature, multiple phases, multiple variables, and unstable states [5]. It differs from other bath smelting processes, such as top-blowing [6] and bottom-blowing [7], in terms of the position of air or oxygen-rich gas injection, reaction conditions, control strategies, and technical indicators. Several factors, including raw material degradation, extensive use of recycled materials, unstable batching, and intensified smelting, lead to variable thermodynamic behaviors in the side-blown furnace during raw material decomposition, melting, oxidation, matte formation, and slagging. These behaviors involve phase transformation, reaction evolution, and component migration and distribution. The current manual and empirical approach faces technical

challenges in quantitatively and directionally controlling these processes, resulting in frequent abnormal furnace conditions such as slag and flue blockage, difficulties in slag–metal separation, increased copper content in slag, accelerated furnace corrosion, and heightened environmental pollution risks [8]. These issues ultimately impact operational efficiency and performance indicators.

In recent years, to overcome the conditional limitations of traditional experimental methods, improve the efficiency of experimental research, and reduce the cost of experimental research, scholars at home and abroad have applied thermodynamic simulation modeling and analysis techniques to pyrometallurgical research on copper, lead, and other metals, achieving research results that can guide production practices. Guo et al. [9,10], Wang et al. [11,12], Li et al. [13,14], and other researchers focused on pyrometallurgical processes such as bottom-blowing copper smelting furnaces and flash smelting furnaces. Based on the principle of multiphase equilibrium, they employed the methods of minimum free energy and chemical equilibrium constant to conduct process optimization analysis on the technological processes after establishing thermodynamic simulation models. On the other hand, Wang et al. [15], Chen et al. [16], Liu et al. [17,18], and others conducted thermodynamic simulation analysis on lead smelting processes such as flash smelting, bottom-blown smelting, and side-blown smelting by establishing a multiphase equilibrium mathematical model based on the method of chemical equilibrium constants. It can be seen that the main thermodynamic simulation modeling and analysis methods for complex pyrometallurgical multiphase reaction systems include the minimum free energy method [19] and the chemical equilibrium constant method [20]. The former has a simple modeling process but lacks satisfactory convergence in solving, while the latter exhibits good convergence and adaptability to trace element systems. However, most existing studies on the copper side-blown smelting process focus on qualitative analysis of the causes of production problems and empirical summaries of improvement measures based on long-term production practices. There is insufficient research on the mechanisms of phase evolution, component migration and distribution, and phase equilibrium analysis during the smelting process. This has led to the inability to quantitatively determine effective control strategies for the complex side-blown oxidative smelting process of copper concentrates. Currently, the main software platforms that can perform thermodynamic simulation modeling and quantitative calculations for copper pyrometallurgical processes include FactSage, HSC Chemistry, Thermal-Cal, MetCal, and others. Among them, the MetCal software platform (MetCal v7.81) is jointly developed by Jiangxi University of Science and Technology and Jiangxi Maikai Technology Co., Ltd. It features comprehensive thermodynamic data and high efficiency in the secondary development of models. Leveraging this platform, it is possible to quickly construct mathematical models for chemical equilibrium, thermal equilibrium, and mass balance in metallurgical and chemical processes. Currently, the MetCal software platform (MetCal v7.81) has been widely used in thermodynamic simulation analysis research on smelting processes of copper, lead, and other metals [21–24].

Because of this, based on the principle of multiphase equilibrium in the copper side-blown smelting process, this article establishes a thermodynamic simulation model and calculation system for the copper side-blown smelting process using the method of chemical equilibrium constants and the MetCal software platform (MetCal v7.81). The model simulates and calculates the composition of products and key technical indicators and compares them with industrial production data to verify the accuracy of the model calculations. This is aimed at providing software tools for subsequent predictions of the process output, revealing the behavior patterns of impurity distribution, and optimizing process parameters.

2. Process Mechanism and Mathematical Model Establishment

2.1. Process Reaction Mechanism

The copper side-blown smelting process is usually under the temperature condition of 1200~1350 °C, blowing oxygen-rich air into the tuyeres on both sides of the copper

side-blown smelting furnace shown in Figure 1. The raw materials, including copper concentrate, flux, reverts, and pulverized coal, are mixed uniformly in a certain proportion and fed into the furnace through a quantitative belt conveyor and feeder from the top of the furnace. The high-speed oxygen-rich air blown into the furnace vigorously agitates the raw materials and melts, creating favorable gas–liquid–solid three-phase heat and mass transfer kinetic conditions, and the particle size of the raw material to be fed into the furnace is generally less than 50 mm. This allows the raw materials to quickly undergo physicochemical evolution processes such as drying, decomposition, melting, slagging, and matte formation. The produced copper melt enters the electric settling furnace through a siphon and chute to complete the clarification and separation of slag and matte, resulting in copper matte and smelting slag. The flue gas generated during the reaction is cooled in a waste heat boiler, and dust is collected in an electric precipitator and then sent to the sulfuric acid system for acid production.

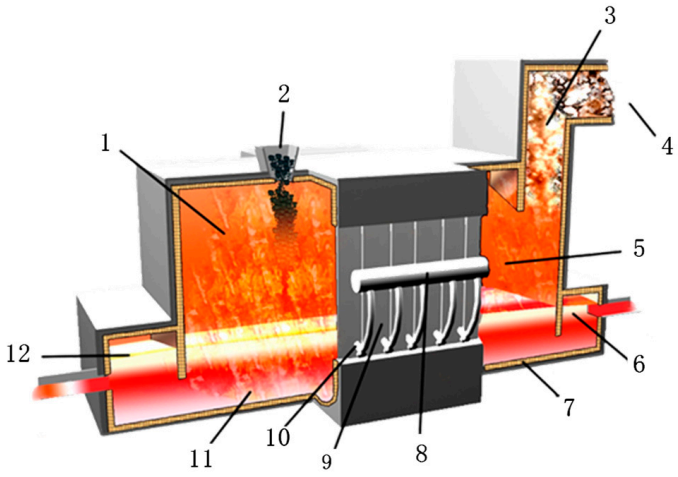

Figure 1. Schematic diagram of copper side-blown smelting furnace. 1—molten pool; 2—feed opening; 3—furnace stack; 4—flue gas; 5—furnace slag; 6—slag basin; 7—fire bricklayer; 8—blast main; 9—sidewall water jacket; 10—tuyere; 11—copper matte; 12—copper matte pool.

The main reactions occurring during the side-blown smelting process of copper concentrate include the decomposition of high-valent sulfides, oxidation of sulfides, matte formation, and slagging.

Decomposition of high-valence sulfides:

$$2FeS_2 = 2FeS + S_2 \quad (1)$$

$$4CuFeS_2 = 2Cu_2S + 4FeS + S_2 \quad (2)$$

Sulfide oxidation:

$$2CuFeS_2 + 4O_2 = Cu_2S + 2FeO + 3SO_2 \quad (3)$$

$$2CuS + O_2 = Cu_2S + SO_2 \quad (4)$$

$$4FeS_2 + 11O_2 = 2Fe_2O_3 + 8SO_2 \quad (5)$$

$$3FeS_2 + 8O_2 = Fe_3O_4 + 6SO_2 \quad (6)$$

Matte formation reaction:

$$FeS + Cu_2O = FeO + Cu_2S \quad (7)$$

$$xFeS + yCu_2S = yCu_2S \cdot xFeS \quad (8)$$

Slagging reaction:

$$2FeS + 3O_2 = 2FeO + 2SO_2 \quad (9)$$

$$2FeO + SiO_2 = 2FeO \cdot SiO_2 \quad (10)$$

Through the above reactions, a copper matte with a higher grade, a smelting slag with a lower copper content, and a suitable slag type, as well as flue gas and dust, can be obtained.

2.2. Modeling Assumption

Based on the reaction mechanism of the copper side-blown smelting process, the products of this process include copper matte, smelting slag, flue gas, and dust. When constructing a multiphase equilibrium model, the equilibrium product phases only include copper matte, smelting slag, and flue gas. Dust is usually considered to be formed by a small amount of unreacted raw materials and fine particle product droplets driven by high-speed airflow in the furnace. Therefore, it is assumed that the composition of dust is consistent with that of a small amount of unreacted raw materials and fine particle product droplets. Based on the above analysis and literature reports, the chemical composition of each product is assumed to be as shown in Table 1. "Other" in the table refers to trace impurity elements, which do not participate in the reaction, but affect the operations involved in modeling the mass conservation relationship.

Table 1. The chemical composition of the product.

Phase	Chemical Components
Copper matte (Mt)	Cu_2S, FeS, FeO, Fe_3O_4, PbS, ZnS, As, Sb, Bi, MoS, Au, Ag_2S, Other1
Smelting slag (Sl)	Cu_2S, Cu_2O, FeS, FeO, Fe_3O_4, SiO_2, CaO, MgO, Al_2O_3, PbO, ZnO, As_2O_3, Sb_2O_3, Bi_2O_3, MoO, Au, Ag, Other2
Flue gas (Gas)	SO_2, SO_3, N_2, O_2, S_2, PbO, PbS, ZnS, ZnO, Zn, AsO, AsS, As_2, SbO, SbS, Sb, BiO, BiS, Bi, CO_2, CO, H_2O
Dust (Dt)	Cu_2S, Cu_2O, FeS, FeO, Fe_3O_4, PbS, PbO, ZnS, ZnO, As_2O_3, As, Sb_2O_3, Sb, Bi, Bi_2O_3, MoS, MoO, Au, Ag, Ag_2S, SiO_2, CaO, MgO, Al_2O_3, Other3

2.3. Model Construction

The copper side-blown smelting process belongs to a multiphase and multicomponent reaction system, and its thermodynamic model can be constructed using the chemical equilibrium constant method [22], also known as the K-value method. This method involves establishing a mathematical model composed of nonlinear equations based on the total molar number of each element in the system and the independent chemical reactions that occur when the system reaches or approaches equilibrium under constant temperature and pressure conditions. The composition of equilibrium products can then be calculated by solving the model.

For any multiphase multicomponent reaction system, assuming that the number of element types is N_e, and the number of chemical species is N_c, all the components of the system can be determined through reactions among the components. Among them, the number of independent reactions N_b is equal to $N_c - N_e$, and the independent reactions can be represented by matrix Equation (11).

$$(V_{j,i})(A_{i,k}) = \left(B_{j,k}\right) \quad (11)$$

In Equation (11), $V_{j,i}$ represents the stoichiometric coefficient matrix, $A_{i,k}$ represents the molecular equation matrix of independent components, and $B_{j,k}$ represents the molecular equation matrix of dependent components. i, j, and k represent the number of independent components, the number of dependent components, and the number of element types, respectively.

According to the rules of matrix operations, this can be obtained through the operation of Equation (12):

$$(V_{j,i}) = \left(B_{j,k}\right)(U_{k,i}) \tag{12}$$

In Equation (12), $U_{k,i}$ is the computable inverse matrix of $A_{j,k}$.

For the copper side-blown smelting reaction system, it is assumed that 20% of the inert elements (components) labeled as "Other" are distributed into the copper matte, inert elements refer to trace impurity elements that do not participate in chemical reactions, such as Se, Te, Pt, etc., while 80% of "Other" elements are distributed into the smelting slag. Based on modeling assumptions and phase equilibrium principles, when constructing a multiphase equilibrium model for the copper side-blown smelting process using the chemical equilibrium constant method, the reaction system includes 19 different elements such as Cu, S, Fe, O, Pb, Zn, As, Sb, Bi, Mo, Ag, Au, Si, Ca, Mg, Al, N, H, and C. There are 51 chemical components in the copper matte, smelting slag, and flue gas products involved in the reaction. The molecular equation matrix of independent chemical components consisting of 19 elements is shown in Appendix A Table A1, while the molecular equation matrix of dependent components consisting of the other 32 dependent chemical components is shown in Appendix A Table A2. Therefore, the number of independent reactions in this reaction system is 32. The chemical reactions and their equilibrium constants K_j of the listed independent components are shown in Table 2. The equilibrium constants of independent reactions can be expressed by Equation (13). In Equations (11) and (12), i ranges from 1 to 19, j ranges from 1 to 32, and k ranges from 1 to 19.

$$K_j = \exp\left(-\frac{\left(\Delta G^0_{bj} - \sum V_{ji}\Delta G^0_{ai}\right)}{RT}\right) \tag{13}$$

Table 2. Independent component reaction and equilibrium constant.

Equilibrium Reaction	K_j	Equilibrium Reaction	K_j
$Cu_2S_{(Mt)} + FeO_{(Mt)} = Cu_2O_{(Sl)} + FeS_{(Sl)}$	K_1	$2CO_{(gas)} + O_{2(gas)} = 2CO_{2(gas)}$	K_{17}
$2FeS_{(Mt)} + 3O_{2(gas)} = 2FeO_{(Sl)} + 2SO_{2(gas)}$	K_2	$2AsS + 2O_{2(gas)} = As_{2(gas)} + 2SO_{2(gas)}$	K_{18}
$FeS_{(Mt)} = FeS_{(Sl)}$	K_3	$As_{2(gas)} + O_{2(gas)} = 2AsO_{(gas)}$	K_{19}
$6FeO_{(Mt)} + O_{2(gas)} = 2Fe_3O_{4(Mt)}$	K_4	$SbS_{(gas)} + O_{2(gas)} = Sb_{(gas)} + SO_{2(gas)}$	K_{20}
$2PbS_{(Mt)} + 3O_{2(gas)} = 2PbO_{(gas)} + 2SO_{2(gas)}$	K_5	$2Sb_{(gas)} + O_{2(gas)} = 2SbO_{(gas)}$	K_{21}
$ZnS_{(Mt)} = ZnS_{(gas)}$	K_6	$BiS_{(gas)} + O_{2(gas)} = Bi_{(gas)} + SO_{2(gas)}$	K_{22}
$2As_{(Mt)} = As_{2(gas)}$	K_7	$2Bi_{(gas)} + O_{2(gas)} = 2BiO_{(gas)}$	K_{23}
$Sb_{(Mt)} = Sb_{(gas)}$	K_8	$2PbS_{(gas)} + 3O_{2(gas)} = 2PbO_{(gas)} + 2SO_{2(gas)}$	K_{24}
$Bi_{(Mt)} = Bi_{(gas)}$	K_9	$ZnS_{(gas)} + O_{2(gas)} = Zn_{(gas)} + SO_{2(gas)}$	K_{25}
$2MoS_{(Mt)} + 3O_{2(gas)} = 2MoO_{(Sl)} + 2SO_{2(gas)}$	K_{10}	$PbO_{(gas)} = PbO_{(Sl)}$	K_{26}
$Au_{(Mt)} = Au_{(Sl)}$	K_{11}	$4AsO_{(gas)} + O_{2(gas)} = 2As_2O_{3(Sl)}$	K_{27}
$Ag_2S_{(Mt)} + O_{2(gas)} = 2Ag_{(Sl)} + SO_{2(gas)}$	K_{12}	$4SbO_{(gas)} + O_{2(gas)} = 2Sb_2O_{3(Sl)}$	K_{28}
$2Cu_2S_{(Sl)} + 3O_{2(gas)} = 2Cu_2O_{(Sl)} + 2SO_{2(gas)}$	K_{13}	$4BiO_{(gas)} + O_{2(gas)} = 2Bi_2O_{3(Sl)}$	K_{29}
$6FeO_{(Sl)} + O_{2(gas)} = 2Fe_3O_{4(Sl)}$	K_{14}	$2Zn_{(gas)} + O_{2(gas)} = 2ZnO_{(Sl)}$	K_{30}
$FeO_{(Sl)} = FeO_{(Mt)}$	K_{15}	$S_{2(gas)} + 2O_{2(gas)} = 2SO_{2(gas)}$	K_{31}
$2SO_{2(gas)} + O_{2(gas)} = 2SO_{3(gas)}$	K_{16}	$2ZnS_{(gas)} + 3O_{2(gas)} = 2ZnO_{(gas)} + 2SO_{2(gas)}$	K_{32}

In Equation (13), R represents the gas constant, T represents the equilibrium temperature of the system, ΔG^0_{ai} represents the standard Gibbs free energy of formation for the i independent component, and ΔG^0_{bi} represents the standard Gibbs free energy of formation for the j dependent component.

When the copper side-blown smelting multiphase reaction system reaches equilibrium, the relationship between its independent components and dependent components can be expressed by Equation (14).

$$Y_j = \left(\frac{Z_{m,j}}{\gamma_j}\right)(K_j)\prod_i\left(\frac{\gamma_i X_i}{Z_{m,i}}\right) \tag{14}$$

In Equation (14), X_i represents the molar quantity of the i independent component, γ_i represents the activity coefficient of the i independent component, Y_j represents the molar quantity of the j dependent component, γ_j represents the activity coefficient of the j dependent component, $Z_{m,i}$ represents the molar quantity of the phase belonging to the i independent component, m represents the product phase, and $Z_{m,j}$ represents the molar quantity of the phase belonging to the j dependent component.

For a closed multiphase reaction system, the mass of each element can be calculated using Equation (15) based on the law of conservation of mass.

$$Q_k = \sum_i A_{i,k}X_i + \sum_j B_{j,k}Y_j \tag{15}$$

In Equation (15), Q_k represents the molar quantity of the element k.

The total molar quantity Z_m of all components in m product phase in Equation (15) can be calculated using Equation (16).

$$Z_m = \sum_{i(m)} X_i + \sum_{j(m)} Y_j \tag{16}$$

In Equation (16), $i(m)$ represents the summation only when the i independent component belongs to the m product phase, and $j(m)$ represents the summation only when the j dependent component belongs to the m product phase.

For the copper side-blown smelting multiphase reaction system, assuming that the number of product phases is N_p, the system temperature, pressure, and the quantities of each element are given and are close to equilibrium, it can be known from Equations (13)–(15) that the system has a total of $(N_c + N_p)$ equations and $(X_i + Y_j + Z_m)$ variables to be solved, with the number of equations equal to the number of variables to be solved. For the thermodynamic simulation model composed of the nonlinear equations from Equations (13)–(16), the Newton–Raphson algorithm and the algorithm flowchart shown in Figure 2 can be used to solve the model, obtaining the molar quantities of each component in the equilibrium products of each phase in the system.

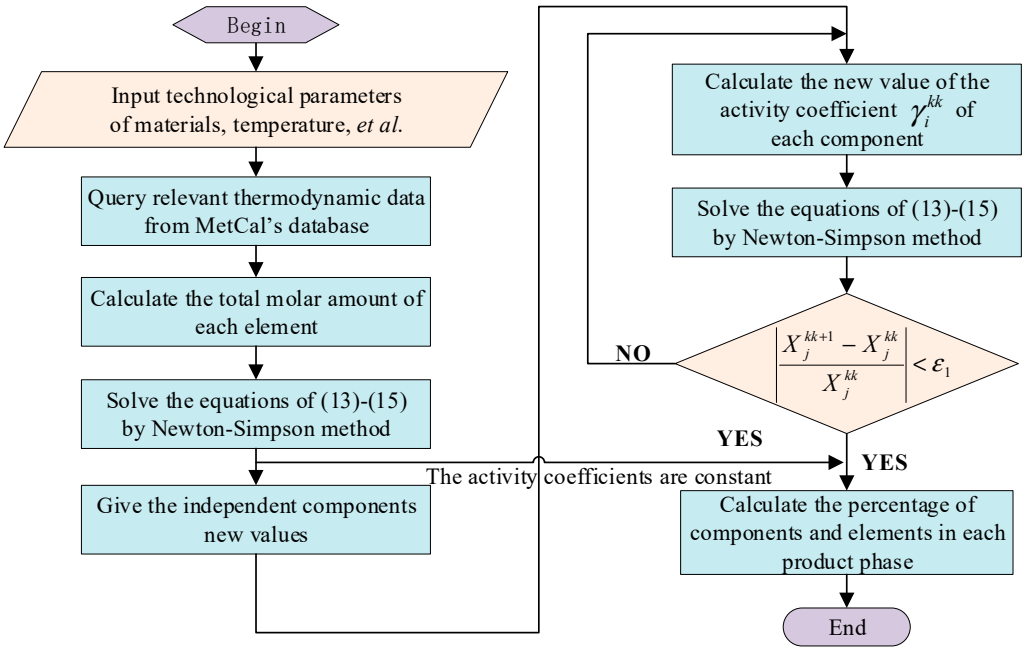

Figure 2. Algorithm calculation process.

3. Basic Data and Digital–Analog System

3.1. Raw Materials and Their Composition

The main raw materials used by a domestic copper side-blown smelting production enterprise include mixed copper concentrate, reverts, burning coal, lime powder, quartz sand, air, and industrial oxygen (with an oxygen volume concentration of 95%). Among them, the mixed copper concentrate is configured from copper concentrates from different origins in proportion, the burning coal is configured from coke powder and anthracite in proportion, and air and industrial oxygen are blown into the furnace through primary and secondary air. The elemental composition of the raw materials used by the enterprise from January to December 2018 was obtained through XRF (X-ray fluorescence spectroscopy) analysis. Combined with the analysis results of the main phases of the raw materials through XRD (phase analysis of X-ray diffraction), the phase calculation models of each raw material were constructed separately based on the MetCal platform (MetCal v7.81), and the phase composition of each raw material was calculated and shown in Tables 3–8. During the detection processes of XRF and XRD, in order to reduce experimental errors, each sample was tested three times, and the average value was taken as the final result.

Table 3. Elemental content of raw materials (wt.%).

Raw Material	Cu	S	Fe	SiO_2	CaO	MgO	Al_2O_3	Pb	Zn	As
Mixed copper concentrate	17.999	22.314	23.583	15.219	1.201	0.889	1.224	0.352	0.770	0.101
Reverts	21.200	10.000	31.037	18.340	2.336	1.240	4.422	-	-	-
Burning coal	-	0.808	0.604	7.179	0.368	0.049	0.200	-	-	-
Limestone	-	-	0.194	4.370	50.768	-	-	-	-	-
Quartz sand	-	-	0.466	88.755	0.970	0.582	0.970	-	-	-
Raw Material	**Sb**	**Bi**	**Mo**	**Au**	**Ag**	**O**	**C**	**H**	**N**	**Other**
Mixed copper concentrate	0.011	0.012	0.159	8.29×10^{-4}	3.90×10^{-3}	11.076	0.522	1.036	-	3.527
Reverts	-	-	-	-	-	6.858	-	-	-	4.566
Burning coal	-	-	-	-	-	4.923	76.405	4.111	1.343	4.011
Limestone	-	-	-	-	-	31.688	10.873	0.336	-	1.770
Quartz sand	-	-	-	-	-	3.418	0.208	0.336	-	4.296

Table 4. Chemical composition of mixed copper concentrate (wt.%).

$CuFeS_2$	Cu_5FeS_4	FeS_2	FeS	SiO_2	$CaCO_3$	$MgCO_3$	Al_2O_3	PbS	ZnS	As_2S_3
32.785	6.708	12.888	4.658	15.219	2.143	1.861	1.224	0.406	1.148	0.166
Sb_2S_3	Bi_2S_3	MoS	Au	Ag_2S	H_2O	FeO	Fe_2O_3	Cu_2O	Other	
0.016	0.014	0.213	0.001	0.004	9.263	4.672	0.385	2.701	3.525	

Table 5. Chemical composition of reverts (wt.%).

Cu_2S	Cu_2O	FeS	FeO	Fe_3O_4	SiO_2	CaO	MgO	Al_2O_3	Other
26.411	0.123	12.834	25.552	4.176	18.34	2.336	1.240	4.422	4.566

Table 6. Chemical composition of burning coal (wt.%).

C	CH_4	CO_2	H_2	N_2	H_2S	Fe_2O_3	SiO_2
75.397	1.2	0.4	3.703	1.343	0.1	0.863	7.179
CaO	MgO	Al_2O_3	H_2O	O_2	S	Other	
0.368	0.049	0.2	0.9	3.573	0.714	4.011	

Table 7. Chemical composition of limestone (wt.%).

$CaCO_3$	FeO	SiO_2	H_2O	Other
90.61	0.25	4.37	3	1.77

Table 8. Chemical composition of quartz sand (wt.%).

SiO_2	Fe_2O_3	$CaCO_3$	Al_2O_3	MgO	H_2O	Other
88.755	0.666	1.731	0.97	0.582	3	4.296

3.2. Thermodynamic Basic Data

Based on the relationship between the standard molar reaction enthalpy and temperature as shown in Equation (17) and the relationship between the standard molar reaction entropy and temperature as shown in Equation (18), the Gibbs free energy of the product components in the copper side-blown smelting process is calculated by Equation (19). The standard thermodynamic parameters of the product components are obtained by querying the MetCal software (MetCal v7.81), as detailed in Appendix A Table A3. To eliminate the influence of reaction kinetics, the activity coefficients of some product phases were corrected based on the results of production sampling analysis and concerning the data reported in the literature. Details are shown in Appendix A Table A4. Among them, MQC indicates that the activity of the component is calculated using the modified quasi-chemical solution activity calculation model provided by MetCal v7.81. It is assumed that the flue gas is ideal; therefore, the activity coefficients of the flue gas components are all 1.

$$\Delta H_T^\theta = \Delta H_{298}^\theta + \int_{298}^{T} C_p \mathrm{d}T \tag{17}$$

$$\Delta S_T^\theta = \Delta S_{298}^\theta + \int_{298}^{T} \frac{C_p}{T} \mathrm{d}T \tag{18}$$

$$\Delta G_T^\theta = \Delta H_{298}^\theta - T \cdot \Delta S_{298}^\theta + \int_{298}^{T} C_p \mathrm{d}T - T \int_{298}^{T} \frac{C_p}{T} \mathrm{d}T \tag{19}$$

3.3. Digital–Analog Computing System

Based on the reaction mechanism of the copper side-blown smelting process and the multiphase equilibrium mathematical model constructed for the copper side-blown smelting process, the thermal equilibrium relationship of this smelting process was established according to the equation shown in Equation (20). The self-developed MetCal software platform (MetCal v7.81) was then utilized to develop a multiphase equilibrium thermodynamic calculation system for the copper side-blown smelting process, as depicted in Figure 3.

$$\sum_{i}^{n_\mathrm{A}} \Delta H_{298,\mathrm{A}_i} + \sum_{i}^{n_\mathrm{A}} \int_{298}^{T_i} Cp_{\mathrm{A}_i} \mathrm{d}T = \sum_{j}^{n_\mathrm{B}} \Delta H_{298,\mathrm{B}_j} + \sum_{j}^{n_\mathrm{B}} \int_{298}^{T_j} C_{p_{\mathrm{B}_j}} \mathrm{d}T + Q_\mathrm{Loss} \tag{20}$$

In Equation (20), A_i is the reactant; T_i is the initial temperature of the reactant A_i; B_j is the product; T_j is the temperature of the product B_j; n_A is the amount of reactant; n_B is the amount of product; H is the enthalpy; C_p is the heat capacity; Q_Loss is the heat loss.

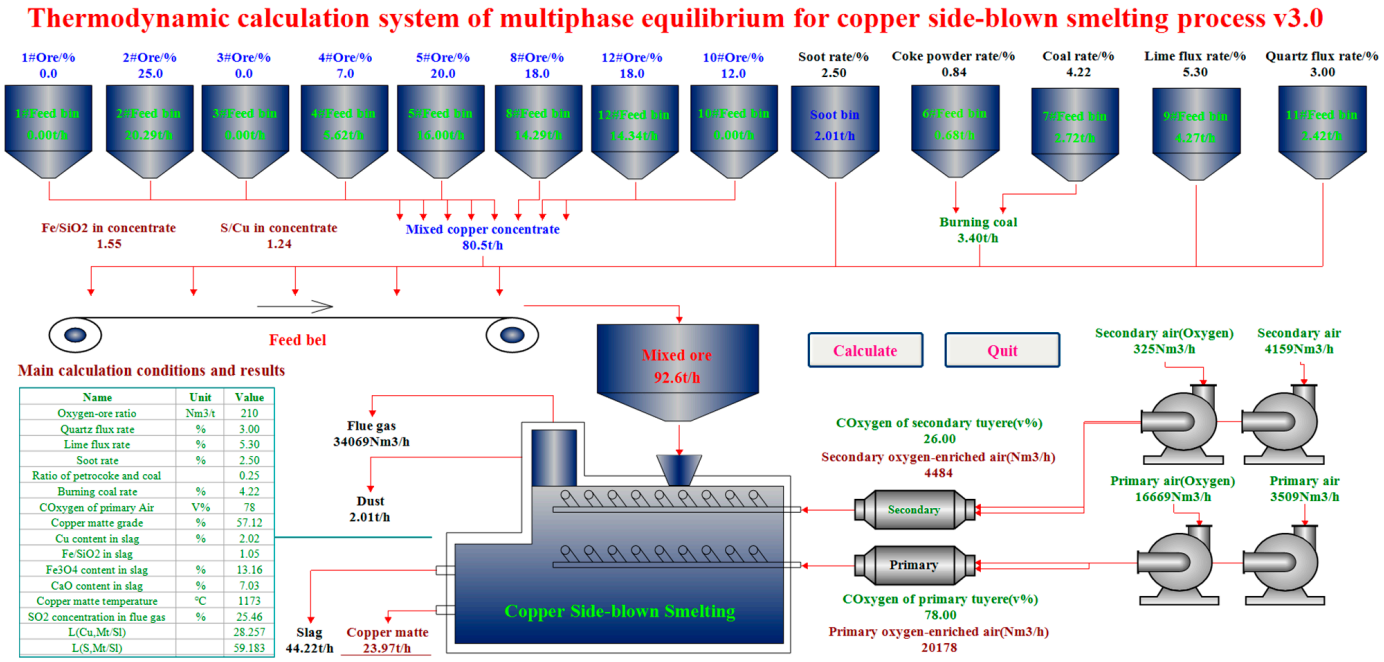

Name	Unit	Value
Oxygen-ore ratio	Nm3/t	210
Quartz flux rate	%	3.00
Lime flux rate	%	5.30
Soot rate	%	2.50
Ratio of petrocoke and coal		0.25
Burning coal rate	%	4.22
COxygen of primary Air	V%	78
Copper matte grade	%	57.12
Cu content in slag	%	2.02
Fe/SiO2 in slag		1.05
Fe3O4 content in slag	%	13.16
CaO content in slag	%	7.03
Copper matte temperature	℃	1173
SO2 concentration in flue gas	%	25.46
L(Cu,Mt/Sl)		28.257
L(S,Mt/Sl)		59.183

Figure 3. Thermodynamic calculation system of multiphase equilibrium for copper side-blown smelting process.

4. Calculation Examples and Model Verification

4.1. Computational Condition

Using the developed multiphase equilibrium thermodynamic calculation system for the copper side-blown smelting process, the composition of the products in the copper side-blown oxidative smelting production process of a domestic copper smelting enterprise was calculated based on the average operating parameters of the side-blown oxidative smelting section of the enterprise from January to December 2018. The total input of raw materials is 92.6 t/h, and the composition of each raw material is described in Section 3.1. Among them, the mixed copper concentrate is 80.5 t/h, the reverts is 2.01 t/h, the burning coal is 3.40 t/h, the limestone is 4.27 t/h, and the quartz sand is 2.42 t/h. The circulating volume of cooling water is 1100 t/h. The oxygen-to-material ratio is 210 Nm^3/t, and the oxygen-rich concentrations of primary air and secondary air are 78% and 26%, respectively. The volume ratio of primary air to secondary air is 4.5. The reverts rate is 2.5%, the burning coal rate is 4.22%, the limestone flux rate is 4.9%, the quartz flux rate is 2.69%, and the smoke dust rate is 1.75%. The temperatures of various smelting products are obtained through thermal balance calculations. It is assumed that the temperature of copper matte is 20 °C lower than that of smelting slag, and the temperature of flue gas and smoke dust is 40 °C higher than that of smelting slag.

4.2. Computation

Under the calculation conditions of the above copper side-blown smelting process, the thermodynamic numerical model and calculation system constructed were used to perform simulation calculations on the process. The chemical composition of copper matte, smelting slag, and dust, as well as the results of thermal balance calculations, are shown in Tables 9–12.

Table 9. Chemical composition of copper matte (wt.%).

Cu_2S	FeS	FeO	Fe_3O_4	PbS	ZnS	As	Sb	Bi	MoS	Au	Ag_2S	Other
71.534	22.111	0.797	0.997	1.036	0.793	0.032	0.008	0.009	0.015	0.003	0.014	2.651

Table 10. Chemical composition of smelting slag (wt.%).

Cu_2S	Cu_2O	FeS	FeO	Fe_3O_4	SiO_2	CaO	MgO	Al_2O_3
1.917	0.552	0.001	32.437	13.164	33.240	7.034	1.655	2.416
PbO	**ZnO**	**As_2O_3**	**Sb_2O_3**	**Bi_2O_3**	**MoO**	**Au**	**Ag**	**Other**
0.146	1.274	0.133	0.018	0.010	0.320	7.44×10^{-5}	3.61×10^{-4}	5.682

Table 11. Chemical composition of dust (wt.%).

Cu_2S	FeS	FeO	Fe_3O_4	PbS	ZnS	As	Sb	Bi
20.018	5.750	24.211	10.000	0.269	0.206	0.008	0.002	0.002
MoS	**Au**	**Ag_2S**	**Cu_2O**	**SiO_2**	**CaO**	**MgO**	**Al_2O_3**	**PbO**
0.004	0.001	0.004	0.409	24.598	5.205	1.225	1.788	0.108
ZnO	**As_2O_3**	**Sb_2O_3**	**Bi_2O_3**	**MoO**	**Ag**	**Other**		
0.943	0.098	0.014	0.007	0.237	0.000	4.894		

Table 12. Heat balance calculation results of copper side-blown smelting process.

Heat Income					Heat Expense				
Heat Type	**Supplies**	**Temp./°C**	**MJ/h**	**%**	**Heat Type**	**Supplies**	**Temp./°C**	**MJ/h**	**%**
Physical heat	Mixed copper concentrate	25	0.00	0.00	Physical heat	Mt	1173	16,873.44	8.26
	Reverts	25	0.00	0.00		Sl	1193	56,541.64	27.70
	Burning coal	25	0.00	0.00		Gas	1233	80,056.76	39.22
	Limestone	25	0.00	0.00		St	1233	1708.54	0.84
	Quartz sand	25	0.00	0.00					
	Primary oxygen	25	0.00	0.00					
	Primary air	25	0.00	0.00					
	Secondary oxygen	25	0.00	0.00					
	Secondary air	25	0.00	0.00					
Chemical heat		25	204,219.43	100.00	Chemical heat		25	0.00	0.00
Exchange heat	Cooling inlet water	39			Exchange heat	Cooling outlet water	45	27,612.06	13.52
					Natural heat dissipation		200	18,807.43	9.21
					Hydrocooling			2500	1.23
Total			204,219.43	100.00	Total			204,219.43	100.00

4.3. Model Verification

In addition to the main elements, the content of impurity elements is one of the important criteria for measuring product quality and is also a key focus in the production process of enterprises, especially the distribution behavior of impurity elements in products such as copper matte and smelting slag. Therefore, to verify the reliability of the constructed model and system, the main element contents and impurity element distribution ratios of products such as copper matte, smelting slag, and smoke dust obtained from simulation calculations were compared with actual production data measured by XRF. The results are listed in Tables 13 and 14 and Figure 4. The error analysis diagram related to the measurement of production value is shown in Figure 5.

Table 13. Comparison of main element content of products with production data (wt.%).

Type	Phase	Cu	S	Fe	SiO_2	CaO	MgO	Al_2O_3
Production data	Mt	57.793	22.420	17.027	0.178	-	-	-
Modeling results		57.124	22.879	15.388	-	-	-	-
Production data	Sl	2.048	0.421	34.643	32.131	7.381	1.821	2.351
Modeling results		2.022	0.387	34.739	33.240	7.034	1.655	2.416

Table 14. Comparison of impurity element distribution ratio of products with production data.

Type	D_x	Pb	Zn	As	Bi	Mo	Au	Ag
Production data	Mt/Sl	6.388	0.498	0.350	1.000	0.039	32.350	32.863
Modeling results		6.628	0.443	0.316	1.081	0.041	34.651	33.647

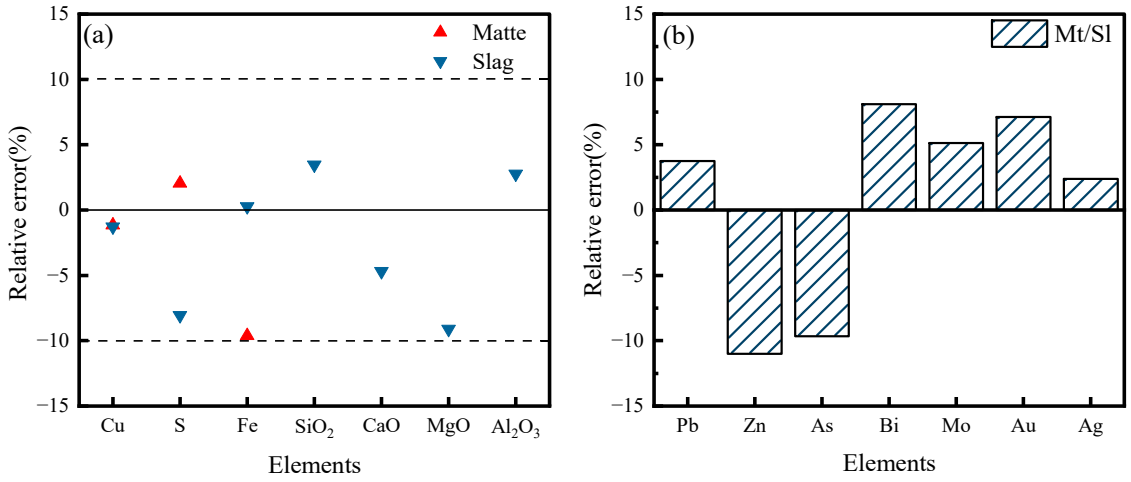

Figure 4. The relative error between the model calculation value and the production data. (**a**) Content of major elements in the product; (**b**) distribution ratio of impurity elements in the product.

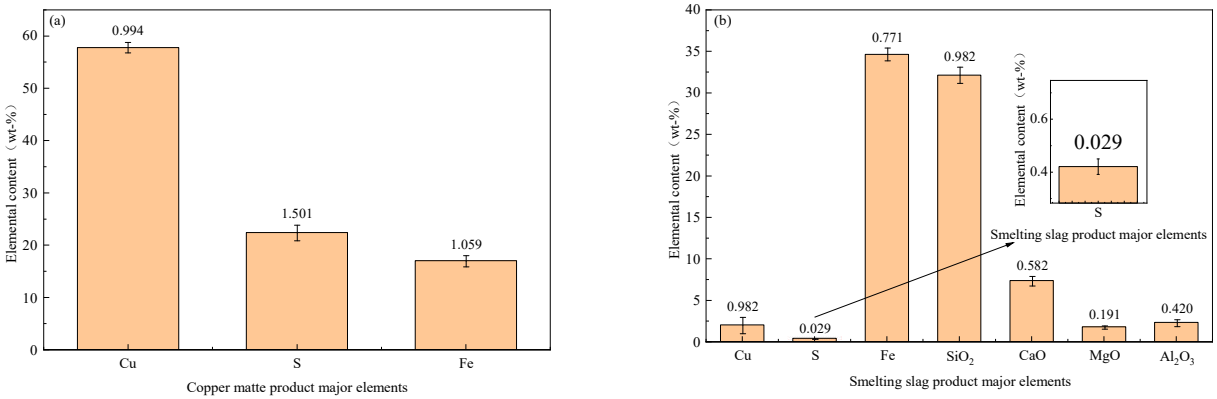

Figure 5. Measurement error of production value. (**a**) Copper matte; (**b**) smelting slag.

According to the results in Tables 13 and 14 and Figure 4, the relative errors between the calculated values and production data for the contents of Cu, S, and Fe in copper matte are 1.16%, 2.05%, and 9.63%, respectively. The relative errors for the contents of Cu, S, Fe, SiO_2, CaO, MgO, and Al_2O_3 (pseudo-elements) in smelting slag are 1.27%, 8.08%, 0.28%, 3.45%, 4.70%, 9.12%, and 2.76%, respectively. The relative errors between the calculated values and production data for the distribution ratios of major impurity elements such as Pb, Zn, As, Bi, Mo, Au, and Ag in copper matte and smelting slag are 3.76%, 11.01%, 9.66%, 8.10%, 5.13%, 7.11%, and 2.39%, respectively. The reasons for these errors may include

inaccuracies in analysis and detection, as well as inherent errors in the model itself. In order to further improve accuracy and reliability, it is still necessary to optimize the model and conduct more precise detection in the future. Although there are certain errors between the production data and calculated values of the model, these errors are currently within a controllable range. This indicates that the distribution behavior of impurity elements in copper matte and smelting slag obtained from simulation calculations is basically consistent with production practice. It can be seen that the established mathematical model can better reflect the thermodynamic reaction mechanism and characteristics of the copper side-blown smelting process and can be used as an analytical tool for subsequently revealing the material evolution and element distribution behavior patterns of the process.

5. Conclusions

1. Based on the reaction mechanism and characteristics of the copper side-blown smelting process, a multiphase equilibrium thermodynamic calculation model was constructed using the method of chemical equilibrium constants. Based on this, a thermodynamic simulation calculation system was developed, providing a software tool for subsequent thermodynamic simulation analysis of the process;
2. Using the constructed model and calculation system, an example validation of the model was conducted based on the typical operating conditions of the copper side-blown smelting process in a domestic enterprise. The calculated results of the products basically matched the production practice, indicating that the model can basically reflect the reaction characteristics of the copper side-blown process and has the potential to predict the refining production process accurately;
3. Through calculation and comparison, it was found that the calculated values of the main element contents and impurity element distribution ratios in the products of the copper side-blown smelting process had small errors compared with the average measured values of production data. The relative errors of the calculated mass fractions of Cu, S, Fe, SiO_2, CaO, MgO, and Al_2O_3 in copper matte and smelting slag are less than 10%. The relative errors of the distribution ratios of impurity elements such as Pb, Zn, As, Bi, Mo, Au, and Ag in copper matte and smelting slag are less than 11.5%. This indicates that the constructed simulation mathematical model can basically reflect the actual production situation of the copper side-blown smelting process and can be used as an effective tool for subsequent systematic thermodynamic analysis of the process.

Author Contributions: Conceptualization, M.L.; methodology, Y.F. and X.C.; formal analysis, Y.F. and X.C.; writing—original draft preparation, M.L. and Y.F.; writing—review and editing, M.L. and X.C.; funding acquisition, M.L. All authors have read and agreed to the published version of the manuscript.

Funding: This research was funded by Project (52364047) supported by the National Natural Science Foundation of China; Project (20212BAB204026) supported by the Natural Science Foundation of Jiangxi Province of China; Project (2019M662268) supported by the China Postdoctoral Science Foundation; Project (2018KY15) supported by the Postdoctoral Funding Program of Jiangxi Province, China; Project (S202210407006) supported by the Innovation and Entrepreneurship Project for College Students of Jiangxi Province, China.

Data Availability Statement: The original contributions presented in the study are included in the article, further inquiries can be directed to the corresponding author.

Acknowledgments: We are very grateful to Jindi Huang, Qiang Chen, Fayou He, and Lihua Zhong for their help with this article. We also appreciate the technical support and industrial samples provided by Chifeng Jintong Copper Industry Co., Ltd. and Zijin Mining Group Co., Ltd.

Conflicts of Interest: Author Mingzhou Li was employed by the Zijin Mining Group Co., Ltd. The remaining authors declare that the research was conducted in the absence of any commercial or financial relationships that could be construed as a potential conflict of interest.

Appendix A

Table A1. Stoichiometry matrix for independent species.

Component	Phase	Cu	S	Fe	O	Pb	Zn	As	Sb	Bi	Mo	Ag	Au	Si	Ca	Mg	Al	N	H	C
Cu_2S	Mt	2	1	0	0	0	0	0	0	0	0	0	0	0	0	0	0	0	0	0
FeS	Mt	0	1	1	0	0	0	0	0	0	0	0	0	0	0	0	0	0	0	0
FeO	Mt	0	0	1	1	0	0	0	0	0	0	0	0	0	0	0	0	0	0	0
Fe_3O_4	Mt	0	0	3	4	0	0	0	0	0	0	0	0	0	0	0	0	0	0	0
PbS	Mt	0	1	0	0	1	0	0	0	0	0	0	0	0	0	0	0	0	0	0
ZnS	Mt	0	1	0	0	0	1	0	0	0	0	0	0	0	0	0	0	0	0	0
As	Mt	0	0	0	0	0	0	1	0	0	0	0	0	0	0	0	0	0	0	0
Sb	Mt	0	0	0	0	0	0	0	1	0	0	0	0	0	0	0	0	0	0	0
Bi	Mt	0	0	0	0	0	0	0	0	1	0	0	0	0	0	0	0	0	0	0
MoS	Mt	0	1	0	0	0	0	0	0	0	1	0	0	0	0	0	0	0	0	0
Ag_2S	Mt	0	1	0	0	0	0	0	0	0	0	2	0	0	0	0	0	0	0	0
Au	Mt	0	0	0	0	0	0	0	0	0	0	0	1	0	0	0	0	0	0	0
SiO_2	Sl	0	0	0	2	0	0	0	0	0	0	0	0	1	0	0	0	0	0	0
CaO	Sl	0	0	0	1	0	0	0	0	0	0	0	0	0	1	0	0	0	0	0
MgO	Sl	0	0	0	1	0	0	0	0	0	0	0	0	0	0	1	0	0	0	0
Al_2O_3	Sl	0	0	0	3	0	0	0	0	0	0	0	0	0	0	0	2	0	0	0
N_2	Gas	0	0	0	0	0	0	0	0	0	0	0	0	0	0	0	0	2	0	0
CO_2	Gas	0	0	0	2	0	0	0	0	0	0	0	0	0	0	0	0	0	0	1
H_2O	Gas	0	0	0	1	0	0	0	0	0	0	0	0	0	0	0	0	0	2	0

Table A2. Stoichiometry matrix for dependent species.

Component	Phase	Cu	S	Fe	O	Pb	Zn	As	Sb	Bi	Mo	Ag	Au	Si	Ca	Mg	Al	N	H	C
Cu_2S	Sl	2	1	0	0	0	0	0	0	0	0	0	0	0	0	0	0	0	0	0
Cu_2O	Sl	2	0	0	1	0	0	0	0	0	0	0	0	0	0	0	0	0	0	0
FeS	Sl	0	1	1	0	0	0	0	0	0	0	0	0	0	0	0	0	0	0	0
FeO	Sl	0	0	1	1	0	0	0	0	0	0	0	0	0	0	0	0	0	0	0
Fe_3O_4	Sl	0	0	3	4	0	0	0	0	0	0	0	0	0	0	0	0	0	0	0
PbO	Sl	0	0	0	1	1	0	0	0	0	0	0	0	0	0	0	0	0	0	0
ZnO	Sl	0	0	0	1	0	1	0	0	0	0	0	0	0	0	0	0	0	0	0
As_2O_3	Sl	0	0	0	3	0	0	2	0	0	0	0	0	0	0	0	0	0	0	0
Sb_2O_3	Sl	0	0	0	3	0	0	0	2	0	0	0	0	0	0	0	0	0	0	0
Bi_2O_3	Sl	0	0	0	3	0	0	0	0	2	0	0	0	0	0	0	0	0	0	0
MoO	Sl	0	0	0	1	0	0	0	0	0	1	0	0	0	0	0	0	0	0	0
Ag	Sl	0	0	0	0	0	0	0	0	0	0	1	0	0	0	0	0	0	0	0
Au	Sl	0	0	0	0	0	0	0	0	0	0	0	1	0	0	0	0	0	0	0
SO_2	Gas	0	1	0	2	0	0	0	0	0	0	0	0	0	0	0	0	0	0	0
SO_3	Gas	0	1	0	3	0	0	0	0	0	0	0	0	0	0	0	0	0	0	0
O_2	Gas	0	0	0	2	0	0	0	0	0	0	0	0	0	0	0	0	0	0	0
S_2	Gas	0	2	0	0	0	0	0	0	0	0	0	0	0	0	0	0	0	0	0
PbO	Gas	0	0	0	1	1	0	0	0	0	0	0	0	0	0	0	0	0	0	0
PbS	Gas	0	1	0	0	1	0	0	0	0	0	0	0	0	0	0	0	0	0	0
ZnS	Gas	0	1	0	0	0	1	0	0	0	0	0	0	0	0	0	0	0	0	0
ZnO	Gas	0	0	0	1	0	1	0	0	0	0	0	0	0	0	0	0	0	0	0
Zn	Gas	0	0	0	0	0	1	0	0	0	0	0	0	0	0	0	0	0	0	0
AsO	Gas	0	0	0	1	0	0	1	0	0	0	0	0	0	0	0	0	0	0	0
AsS	Gas	0	1	0	0	0	0	1	0	0	0	0	0	0	0	0	0	0	0	0
As_2	Gas	0	0	0	0	0	0	2	0	0	0	0	0	0	0	0	0	0	0	0
SbO	Gas	0	0	0	1	0	0	0	1	0	0	0	0	0	0	0	0	0	0	0
SbS	Gas	0	1	0	0	0	0	0	1	0	0	0	0	0	0	0	0	0	0	0
Sb	Gas	0	0	0	0	0	0	0	1	0	0	0	0	0	0	0	0	0	0	0
BiO	Gas	0	0	0	1	0	0	0	0	1	0	0	0	0	0	0	0	0	0	0
BiS	Gas	0	1	0	0	0	0	0	0	1	0	0	0	0	0	0	0	0	0	0
Bi	Gas	0	0	0	0	0	0	0	0	1	0	0	0	0	0	0	0	0	0	0
CO	Gas	0	0	0	1	0	0	0	0	0	0	0	0	0	0	0	0	0	0	1

Table A3. Standard thermodynamic parameters of product components.

Component	State	ΔH^{Θ}_{298}/ (kJ·mol^{-1})	ΔS^{Θ}_{298}/ (J·K^{-1}·mol^{-1})	$C_p = a + b\times10^{-3}T + c\times10^{5}T^{-2} + d\times10^{-6}T^{2}$			
				a	b	c	d
Cu_2S	Liquid	−68.100	132.462	89.665	0.000	0.000	0.000
Cu_2O	Liquid	−130.224	96.402	99.916	0.000	0.000	0.000
FeS	Liquid	−64.631	91.208	62.552	0.000	0.000	0.000
FeO	Liquid	−257.276	57.591	68.201	0.000	0.000	0.000
Fe_3O_4	Liquid	−993.334	198.385	213.389	0.000	0.000	0.000
SiO_2	Liquid	−927.548	9.310	85.774	0.000	0.000	0.000
CaO	Liquid	−572.908	40.980	62.762	0.000	0.000	0.000
MgO	Liquid	−561.018	12.833	66.946	0.000	0.000	0.000
Al_2O_3	Liquid	−595.568	45.145	144.866	0.000	0.000	0.000
PbS	Liquid	−93.143	84.129	66.946	0.000	0.000	0.000
PbO	Liquid	−202.249	73.379	65.000	0.000	0.000	0.000
ZnS	Liquid	−203.005	58.661	67.002	0.000	0.000	0.000
ZnO	Liquid	−309.542	47.920	60.669	0.000	0.000	0.000
As	Liquid	21.568	53.284	28.833	0.000	0.000	0.000
As_2O_3	Liquid	−643.439	128.135	152.720	0.000	0.000	0.000
Sb	Liquid	17.531	62.712	31.381	0.000	0.000	0.000
Sb_2O_3	Liquid	−675.490	143.628	156.904	0.000	0.000	0.000
Bi	Liquid	9.271	71.980	27.197	0.000	0.000	0.000
Bi_2O_3	Liquid	−578.024	149.814	202.005	0.000	0.000	0.000
MoS	Liquid	−407.113	114.979	156.904	0.000	0.000	0.000
MoO	Liquid	358.015	302.620	38.457	−1.797	−0.517	0.825
Au	Liquid	0.000	47.489	−268.634	237.139	1418.47	−52.813
Ag	Liquid	6.393	43.220	33.473	0.000	0.000	0.000
Ag_2S	Liquid	−32.791	142.893	93.002	0.000	0.000	0.000
SO_2	Gas	−296.820	248.226	54.781	3.350	−24.745	−0.241
SO_3	Gas	−395.774	256.778	77.834	4.032	−42.617	−0.369
N_2	Gas	0.000	191.615	35.369	1.041	−41.465	0.111
O_2	Gas	0.000	205.154	34.860	1.312	−14.141	0.163
S_2	Gas	128.603	228.169	34.672	3.286	−2.816	−0.312
CO_2	Gas	−393.515	213.774	54.437	5.116	−43.579	−0.806
CO	Gas	−110.544	197.665	29.932	5.415	−10.814	−1.054
H_2O	Gas	−241.832	188.837	31.438	14.106	−24.952	−1.832
PbS	Gas	127.959	251.416	37.350	0.194	−2.096	0.140
PbO	Gas	68.139	240.048	41.612	−3.526	−20.136	1.014
ZnS	Gas	204.322	236.404	27.713	7.021	251.297	−1.105
ZnO	Gas	136.518	242.811	37.671	−0.286	−1.954	0.735
Zn	Gas	130.403	160.992	20.898	−0.133	−0.067	0.034
AsO	Gas	43.807	230.408	43.664	−4.280	−11.197	0.946
AsS	Gas	181.400	242.065	44.417	−4.409	−6.808	0.916
As_2	Gas	190.711	240.888	36.702	1.152	−1.774	−0.507
SbO	Gas	−103.502	238.351	47.257	−3.650	−40.324	0.512
SbS	Gas	190.794	249.701	46.218	−2.657	−34.352	0.255
Sb	Gas	267.181	180.273	8.955	6.151	80.063	−0.315
BiO	Gas	125.690	246.413	36.508	0.526	−3.663	0.001
BiS	Gas	176.552	257.878	38.237	−1.090	−3.599	0.765
Bi	Gas	208.742	187.011	21.189	−0.732	−0.203	0.320

Table A4. Activity coefficients of product components.

Component	Product	Activity Coefficient	References
Cu_2S	Mt	1	[25–27]
FeS	Mt	$0.925/(x_{Cu_2S}+1)$	[25]
FeO	Mt	$\exp[5.1+6.2(\ln x_{Cu_2S})+6.4(\ln x_{Cu_2S})^2+2.8(\ln x_{Cu_2S})^3]$	[25]
Fe_3O_4	Mt	$\exp[4.96+9.9(\ln x_{Cu_2S})+7.43(\ln x_{Cu_2S})^2+2.55(\ln x_{Cu_2S})^3]$	[25]
PbS	Mt	$\exp[-2.716+2441/T+(0.815-3610/\mathrm{T})(80-[\mathrm{Pct}\cdot Cu]_{\mathrm{mt}})/100]$	[25]
ZnS	Mt	$\exp[-2.054+6917/T-(1.522-1032/\mathrm{T})(80-[\mathrm{Pct}\cdot Cu]_{\mathrm{mt}})/100]$	[25]
As	Mt	$\exp((2180+3093(80-[\mathrm{Pct}\cdot Cu]_{\mathrm{mt}})/100)/T)$	[28]
Sb	Mt	$\exp((4478+3388(80-[\mathrm{Pct}\cdot Cu]_{\mathrm{mt}})/100)/T)$	[28]
Bi	Mt	$\exp(1900/T-0.885)$	[29]
MoS	Mt	MQC	Activity model
Au	Mt	$10^{(-3310/T+3.15)}$	[30,31]
Ag_2S	Mt	$10^{(-425/T-0.074+0.09x_{FeS})}$	[30,31]
Cu_2O	Sl	$57.14x_{Cu_2O}$	[25]
Cu_2S	Sl	$\exp(2.46+6.22N_{Cu_2S(mt)})$	[25]
FeS	Sl	70	[25]
FeO	Sl	$1.42x_{FeO}-0.044$	[25]
Fe_3O_4	Sl	$0.69+56.8x_{Fe_3O_4}+5.45x_{SiO_2}$	[25]
SiO_2	Sl	2.1	[32]
CaO	Sl	1	[32]
MgO	Sl	1	[32]
Al_2O_3	Sl	1	[32]
PbO	Sl	$\exp(-3926/T)$	[30]
ZnO	Sl	$\exp(400/T)$	[33]
As_2O_3	Sl	$3.838\exp(1523/T)\cdot P_{O_2}^{0.158}$	[30]
Sb_2O_3	Sl	$\exp(1055.66/T)$	[30]
Bi_2O_3	Sl	$\exp(-1055.66/T)$	[30]
MoO	Sl	MQC	Activity model
Au	Sl	480	[31,34]
Ag	Sl	920	[31,35]

References

1. Hu, Z.Y. Design and Application of Oxygen Enriched Side Blowing for Copper Smelting Process Control System. *South. Met.* **2023**, 9–12+29. [CrossRef]
2. Yuan, J.H. Current Status and Outlook of Side Blowing Furnace. *Nonferrous Met. (Extr. Metall.)* **2022**, 31–35. [CrossRef]
3. Yang, B.; Liu, W.; Jiao, F.; Zhang, L.; Qin, W.; Jiang, S. Numerical Simulation and Application of an Oxygen-Enriched Side-Blown Smelting Furnace for the Treatment of Electroplating Sludge. *Sustainability* **2023**, *15*, 10721. [CrossRef]
4. Xie, S.; Zhao, B. Phase Equilibrium Studies of Nonferrous Smelting Slags: A Review. *Metals* **2024**, *14*, 278. [CrossRef]
5. Zou, Q.; Hu, J.; Yang, S.; Wang, H.; Deng, G. Investigation of the Splashing Characteristics of Lead Slag in Side-Blown Bath Melting Process. *Energies* **2023**, *16*, 1007. [CrossRef]
6. Zhao, B.; Ren, Y.Z.; Jia, W.L.; Zhang, Y.Y.; Zhou, S.W.; Li, B. Regulation of arsenic element trend in copper top-blown smelting process. *China Nonferrous Metall.* **2024**, *53*, 88–97. [CrossRef]
7. Wang, W.; Cai, X.; Mu, L.; Lu, T.; Lv, C.; Zhao, H.; Sohn, H.Y. CFD Simulation of the Effects of Mushroom Heads in a Bottom-Blown Copper Smelting Furnace. *Metall. Mater. Trans. B-Proc. Metall. Mater. Proc. Sci.* **2024**, *55*, 694–708. [CrossRef]
8. Shi, L.; Wang, Z.Y. Analyzing the Factors Affecting the Concentration of Dilute Acid in the Copper Smelting Process of Oxygen-rich Side Blowing Furance. *Non-Ferr. Min. Metall.* **2024**, *40*, 31–33.
9. Guo, X.Y.; Wang, Q.M.; Tian, Q.H.; Zhang, Y.Z. Non-steady multiphase equilbrium process of copperoxygen-enriched bottom blowing bath smelting with gradual changeof oxygen and sulfur potential of different positions in furance. *Chin. J. Nonferrous Met.* **2015**, *25*, 1072–1079. [CrossRef]
10. Guo, X.Y.; Wang, Q.M.; Tian, Q.H.; Zhao, B.J. Analysis and optimization of oxygen bottomblowing copper smelting process. *Chin. J. Nonferrous Met.* **2016**, *26*, 689–698. [CrossRef]
11. Wang, Q.; Guo, X.; Tian, Q.; Jiang, T.; Chen, M.; Zhao, B. Development and Application of SKSSIM Simulation Software for the Oxygen Bottom Blown Copper Smelting Process. *Metals* **2017**, *7*, 431. [CrossRef]
12. Wang, Q.; Guo, X.; Tian, Q.; Jiang, T.; Chen, M.; Zhao, B. Effects of Matte Grade on the Distribution of Minor Elements (Pb, Zn, As, Sb, and Bi) in the Bottom Blown Copper Smelting Process. *Metals* **2017**, *7*, 502. [CrossRef]

13. Li, M.; Zhou, J.; Tong, C.; Zhang, W.; Chen, Z.; Wang, J. Thermodynamic Modeling and Optimization of the Copper Flash Converting Process Using the Equilibrium Constant Method. *Metall. Mater. Trans. B-Proc. Metall. Mater. Proc. Sci.* **2018**, *49*, 1794–1807. [CrossRef]
14. Li, M.Z.; Zhou, J.M.; Zhang, W.H.; Li, H.S.; Tong, C.R. Thermodynamics analysis of distribution behavior of impurity elements during copper flash converting. *Chin. J. Nonferrous Met.* **2017**, *27*, 1951–1959. [CrossRef]
15. Wang, J.L.; Zhang, C.F.; Zhang, W.H. Multi-phase equilibrium model of lead flash smelting process. *J. Cent. South Univ. (Sci. Technol.)* **2012**, *43*, 429–434.
16. Chen, L.; Yang, T.Z.; Liu, W.F.; Zhang, D.C.; Bin, S.; Bin, W.D. Distribution of valuable metals in liquid high lead slag during reduction process. *Chin. J. Nonferrous Met.* **2014**, *24*, 1056–1062. [CrossRef]
17. Liu, Y.T.; Yang, T.Z.; Li, M.Z. Phase equilibrium model for lead oxygen-enriched side-blown oxidation bath smelting. *Chin. J. Nonferrous Met.* **2019**, *29*, 2609–2619. [CrossRef]
18. Liu, Y.T.; Yang, T.Z.; Li, M.Z. Multielement and multiphase equilibrium analysis of lead oxygen-enriched side-blown oxidation smelting. *Chin. J. Nonferrous Met.* **2020**, *30*, 1110–1118.
19. Shen, Z.; Li, Y.; Xu, N.; Sun, B.; Du, W.; Xu, M.; Chang, L. Investigation on the Chemical Equilibrium Products for $C_nH_mO_lN_k$ Type Fuels Using Equilibrium Constants Database. *Fuel* **2022**, *310*, 122325. [CrossRef]
20. Ye, Z.L.; Zhu, Y.F.; Zhang, H.P.; Zhou, S.W.; Li, B.; Shi, Z. A Thermodynamic Study of Copper Oxygen-Riched Smelting Process to Produce High-Grade Matte. *J. Kunming Univ. Sci. Technol. (Nat. Sci.)* **2022**, *47*, 54. [CrossRef]
21. Xu, S.C.; Li, M.Z.; Zhao, Z.H.; Zhong, L.H.; He, F.Y.; Huang, J.D. Thermodynamic simulation modeling of copper anode furnace refining process based on MetCal software. *Chin. J. Nonferrous Met.* **2024**, 1–21. [CrossRef]
22. Chen, X.; Li, M.; Liu, F.; Huang, J.; Yang, M. Multi-Phase Equilibrium Model of Oxygen-Enriched Lead Oxidation Smelting Process Based on Chemical Equilibrium Constant Method. *Processes* **2023**, *11*, 3043. [CrossRef]
23. Lin, L.; He, F. Numerical Simulation Whole Process of Oxygen-Enriched Side-Blown Smelting and Multi-Lance Top-Blown Converting. *Nonferrous Met. (Extr. Metall.)* **2023**, 103–112. [CrossRef]
24. Xiao, Y.; Lu, T.; Zhou, Y.; Su, Q.; Mu, L.; Wei, T.; Zhao, H.; Liu, F. Computational Fluid Dynamics Study on Enhanced Circulation Flow in a Side-Blown Copper Smelting Furnace. *JOM* **2021**, *73*, 2724–2732. [CrossRef]
25. Tan, P.F.; Zhang, C.F. Computer Model of Distribution Behavior of Accessory Elements in Copper Smelting. *Acta Metallurgica Sinica* **1997**, *10*, 1094–1100. [CrossRef]
26. Shimpo, R. An Application of Equibibrium Calculations to the Copper Smelting Operation. Available online: https://onemine.org/documents/an-application-of-equibibrium-calculations-to-the-copper-smelting-operation (accessed on 23 April 2024).
27. Shimpo, R.; Goto, S.; Ogawa, O.; Asakura, I. A Study on the Equilibrium between Copper Matte and Slag. *Can. Metall. Q.* **1986**, *25*, 113–121. [CrossRef]
28. Nagamori, M.; Errington, W.J.; Mackey, P.J.; Poggi, D. Thermodynamic Simulation Model of the Isasmelt Process for Copper Matte. *Met. Mater. Trans. B* **1994**, *25*, 839–853. [CrossRef]
29. Nagamori, M.; Mackey, P.J.; Tarassoff, P. Copper Solubility in $FeO-Fe_2O_3-SiO_2-Al_2O_3$ Slag and Distribution Equilibria of Pb, Bi, Sb and As between Slag and Metallic Copper. *Met. Trans. B* **1975**, *6*, 295–301. [CrossRef]
30. Tan, P.; Zhang, C. Computer Model of Copper Smelting Process and Distribution Behaviors of Accessory Elements. *J. Cent. South Univ. Technol.* **1997**, *4*, 36–41. [CrossRef]
31. Sinha, S.N.; Sohn, H.Y.; Nagamori, M. Distribution of Gold and Silver between Copper and Matte. *Met. Trans. B* **1985**, *16*, 53–59. [CrossRef]
32. Swinbourne, D.R.; Kho, T.S. Computational Thermodynamics Modeling of Minor Element Distributions During Copper Flash Converting. *Metall. Mater. Trans. B-Proc. Metall. Mater. Proc. Sci.* **2012**, *43*, 823–829. [CrossRef]
33. Mackey, P.J. The Physical Chemistry of Copper Smelting Slags—A Review. *Can. Metall. Q.* **1982**, *21*, 221–260. [CrossRef]
34. Hall, L.D. The Vapor Pressure of Gold and the Activities of Gold in Gold-Copper Solid Solutions. *J. Am. Chem. Soc.* **1951**, *73*, 757–760. [CrossRef]
35. Swinbourne, D.R.; Yazawa, A.; Barbante, G.G. Thermodynamic Modeling of Selenide Matte Converting. *Met. Mater. Trans. B* **1997**, *28*, 811–819. [CrossRef]